Remote Sensing of Environment xxx (2008) xxx–xxx

Contents lists available at ScienceDirect

Remote Sensing of Environment

journal homepage: www.elsevier.com/locate/rse

Generating vegetation leaf area index earth system data record from multiple sensors. Part 1: Theory

Sangram Ganguly [a,*], Mitchell A. Schull [a], Arindam Samanta [a], Nikolay V. Shabanov [b], Cristina Milesi [c], Ramakrishna R. Nemani [c], Yuri Knyazikhin [a], Ranga B. Myneni [a]

[a] Department of Geography and Environment, Boston University, 675 Commonwealth Avenue, Boston, MA 02215, USA
[b] NOAA/NESDIS, 5200 Auth Rd., Camp Springs, MD 20746, USA
[c] Ecosystem Science and Technology Branch, NASA Ames Research Center, Mail Stop 242-4, Mofett Field, CA 94035, USA

ARTICLE INFO

Article history:
Received 28 February 2008
Received in revised form 28 July 2008
Accepted 29 July 2008
Available online xxxx

Keywords:
Leaf area index
Spectral invariant
Recollision probability
Radiative transfer
Long-term data record
AVHRR
MODIS
Scaling
Single scattering albedo
Data uncertainties

ABSTRACT

The generation of multi-decade long Earth System Data Records (ESDRs) of Leaf Area Index (LAI) and Fraction of Photosynthetically Active Radiation absorbed by vegetation (FPAR) from remote sensing measurements of multiple sensors is key to monitoring long-term changes in vegetation due to natural and anthropogenic influences. Challenges in developing such ESDRs include problems in remote sensing science (modeling of variability in global vegetation, scaling, atmospheric correction) and sensor hardware (differences in spatial resolution, spectral bands, calibration, and information content). In this paper, we develop a physically based approach for deriving LAI and FPAR products from the Advanced Very High Resolution Radiometer (AVHRR) data that are of comparable quality to the Moderate resolution Imaging Spectroradiometer (MODIS) LAI and FPAR products, thus realizing the objective of producing a long (multi-decadal) time series of these products. The approach is based on the radiative transfer theory of canopy spectral invariants which facilitates parameterization of the canopy spectral bidirectional reflectance factor (BRF). The methodology permits decoupling of the structural and radiometric components and obeys the energy conservation law. The approach is applicable to any optical sensor, however, it requires selection of sensor-specific values of configurable parameters, namely, the single scattering albedo and data uncertainty. According to the theory of spectral invariants, the single scattering albedo is a function of the spatial scale, and thus, accounts for the variation in BRF with sensor spatial resolution. Likewise, the single scattering albedo accounts for the variation in spectral BRF with sensor bandwidths. The second adjustable parameter is data uncertainty, which accounts for varying information content of the remote sensing measurements, i.e., Normalized Difference Vegetation Index (NDVI, low information content), vs. spectral BRF (higher information content). Implementation of this approach indicates good consistency in LAI values retrieved from NDVI (AVHRR-mode) and spectral BRF (MODIS-mode). Specific details of the implementation and evaluation of the derived products are detailed in the second part of this two-paper series.

© 2008 Elsevier Inc. All rights reserved.

1. Introduction

The monitoring and modeling of the terrestrial biosphere within the larger context of climate variability and change studies requires multi-decadal time series of key variables characteristic of vegetation structure and functioning (NRC Decadal Survey, 2007; GCOS, 2006). Consequently, there is now a pressing need to develop methodologies for generating continuous long-term Earth System Data Records (ESDRs) from remote sensing data collected with different sensors over the past three decades. In this article, we focus on two key biophysical variables, leaf area index (LAI) and fraction vegetation absorbed photosynthetically active radiation (FPAR), that control the exchange of energy, mass (e.g. water and CO_2) and momentum between the Earth surface and atmosphere (Dickinson et al., 1986; Potter et al., 1993; Sellers et al., 1996; Tian et al., 2004; Demarty et al., 2007).

The Advanced Very High Resolution Radiometers (AVHRR) onboard NOAA 7-14 series satellite platforms delivered the first high temporal resolution global time series of data suitable for vegetation sensing starting from July 1981 (Tucker et al., 2005). The NASA Moderate Resolution Imaging Spectroradiometer (MODIS) and Multi-angle Imaging SpectroRadiometer (MISR) onboard Terra and Aqua platforms started providing higher quality spectral and angular measurements since February 2000 (Diner et al., 1999; Justice & Townshend, 2002). These records are expected to be extended by the planned Visible/Infrared Imager Radiometer Suite (VIIRS) instrument onboard the NPOESS Preparatory Project (NPP) to be launched in the near future

* Corresponding author. Tel.: +1 617 319 6249; fax: +1 617 353 8399.
E-mail address: sganguly@bu.edu (S. Ganguly).

0034-4257/$ – see front matter © 2008 Elsevier Inc. All rights reserved.
doi:10.1016/j.rse.2008.07.014

(Murphy, 2006). Other long-term sources of data for vegetation monitoring include the Sea-viewing Wide Field-of-view Sensor (SeaWiFS), Systeme Pour l'Observation de la Terre (SPOT) VEGETATION, and ENVISAT Medium Resolution Imaging Spectrometers (MERIS).

The challenges underlying the generation of continuous time series of land products from data of multiple instruments include both remote sensing science and sensor-related issues. The scientific challenges include modeling highly variable radiative properties of global vegetation, scaling, and atmospheric correction of data. Traditionally, the Normalized Difference Vegetation Index (NDVI) has been used for long-term global vegetation monitoring (Myneni et al., 1997). Biophysical parameters (LAI and FPAR) have been retrieved from NDVI using empirical relationships (Sellers et al., 1996). However, those relationships are site-, time-, and biome-specific and their use in global operational production may be limited (Baret & Guyot, 1991; Wang et al., 2004). Scaling issues (mixture of different vegetation types) introduce an additional bias as vegetation classes with relatively low pixel fractional coverage are under-represented in coarse resolution retrievals (Tian et al., 2002; Steltzer & Welker, 2006; Shabanov et al., 2007). Finally, the retrieval of biophysical parameters require surface reflectances, however, a complete atmospheric correction of AVHHR data was not performed in the past due to limited availability of requisite ancillary data.

The hardware issues include differences in sensor spectral characteristics, spatial resolution, calibration, measurement geometry and data information content. Differences in sensor spectral bands (central wavelength and bandwidth) result in differential sensitivity of the sensor's spectral response functions (SRF) to the impact of Rayleigh scattering, ozone, aerosol optical thickness, water vapor content and reflection from the ground (Vermote & Saleous, 2006; Van Leeuwen et al., 2006). The variation in spatial resolution involves the impact of sensor-dependent Point Spread Function (PSF), such that radiometric measurements for a particular pixel are partially mixed with those of adjacent pixels and re-sampling to the common resolution almost always results in a bias (Tan et al., 2006). At- and post-calibration results in varying sensitivity of satellite image Digital Numbers (DN) to recorded radiation (Vermote & Saleous, 2006). The calibration issues are further complicated by orbital drift and related changes in illumination/observation geometry (Gutman, 1998). Finally, the information content of measurements will vary between sensors, e.g. due to different number of bands, view angles, etc., and retrieval techniques should take advantage of available multi-angular, multi-spectral, high spatial or temporal resolution measurements.

The two widely used NDVI time series data are the Pathfinder AVHRR Land (PAL) and Global Inventory Monitoring and Modeling Studies (GIMMS) (Tucker et al., 2005). These data sets cover nearly the entire record (July 1981 to the present) at 8-km spatial resolution as 15-day temporal composites (PAL is 10-day composite). The data processing included calibration, interpolation of missing data, and partial atmospheric correction with statistical techniques. Several studies reveal significant trends in NDVI over the Northern high latitudes (Myneni et al., 1997; Zhou et al., 2001); however, the accuracy of the assessment was questioned (Gutman, 1998). The Canadian Center for Remote Sensing is routinely generating Canada-wide time series of LAI and FPAR from AVHRR and VEGETATION at 1-km resolution as 10-day composites using empirical algorithms (Chen et al., 2002). Likewise, the Joint Research Center is currently developing time series of FPAR from SeaWiFS, MERIS, and VEGETATION (Gobron et al., 2006).

Multi-decadal global data sets of LAI and FPAR of known accuracy and produced with a physically based algorithm are currently not available. Efforts are underway to perform rigorous physically based calibration and atmospheric correction to achieve consistency with the reference MODIS NDVI records (Vermote & Saleous, 2006). These efforts should result in higher quality surface reflectance data ideally suited for producing LAI and FPAR ESDRs. Thus, the objectives of this research are to formulate and demonstrate the performance of a synergistic approach for LAI and FPAR ESDR retrievals from measurements of multiple satellite sensors. The theoretical aspects of the approach are presented in this paper, while results from evaluation of the quality of the generated data series are presented in the second paper. This paper is organized as follows. The criteria for ensuring consistency between retrievals from different sensors are formulated in Section 2. The next section introduces the theoretical basis of a multi-sensor retrieval algorithm, namely, parameterization of the canopy spectral reflectance using the radiative transfer theory of spectral invariants. Methods for accounting differences in sensor spatial resolution and spectral bands are presented in Sections 4 and 5. The following section describes an approach to adjust the retrieval technique for handling variations in the information content of the satellite data. Finally, the concluding remarks are given in Section 7.

2. Criteria for ensuring consistency

Generation of ESDRs from observations of multiple instruments requires deriving an inter-sensor consistent product which also matches well with ground truth measurements. A one-to-one relationship between remote observations and a land parameter of interest can be achieved only in the case of error-free measurements delivering sufficient information content (Choulli & Stefanov, 1996). In practice, the retrieval of LAI and FPAR from satellite data should be treated as an ill-posed problem; that is, small variations in input data due to uncertainties in measurements can result in a change in the relationship, leading not only to non-physically high variations in the retrieved values but also to the loss of a true solution, since it may not satisfy the altered relationship (Wang et al., 2001; Combal et al., 2002; Tan et al., 2005). Input data and their uncertainties are, “in general, the minimal information necessary to construct approximate solution for ill-posed problems” (Tikhonov et al., 1995, p.3). The inclusion of more measured information (spectral and/or angular variation) tends to improve the relationship between satellite observations and the desired parameters. This however not only increases the overall data information content but also increases their overall uncertainty. The former enhances the quality of retrievals while the latter suppresses it. Therefore, the specification of an optimal combination of data information content and overall uncertainty is a key task to achieving continuity in the multi-sensor time series of LAI and FPAR products.

In general, the information conveyed by surface reflectances is not sufficient to retrieve a unique LAI value. For example, different combinations of LAI and soil types can result in the same value of canopy spectral reflectances; or different spectral reflectances can correspond to the same LAI value but for different vegetation types (Diner et al., 2005). A particular observation of surface reflectance is therefore associated with a set of canopy parameter values. We refer to these as the set of acceptable solutions (Knyazikhin et al., 1998a). This set of solutions depends on the properties of measured surface reflectances: absolute values and uncertainties, spectral characteristics, spatial resolution, and observation geometry. In general, a larger volume and higher accuracy of the measured information corresponds to a better localized set of solutions. The solution set “size” can, therefore, be used as a measure of the data information content. We use this concept to formulate the following requirements for a multi-sensor algorithm to generate consistent LAI and FPAR retrievals from AVHRR and MODIS sensors:

(a) The algorithm should generate a set of acceptable solutions given AVHRR NDVI;
(b) This set should include all acceptable solutions generated by the MODIS algorithm when given the corresponding AVHRR spectral reflectances;
(c) The algorithm should also be capable of admitting AVHRR spectral reflectances, in addition to NDVI, and generate the same set of acceptable solutions as the MODIS algorithm.

Please cite this article as: Ganguly, S., et al., Generating vegetation leaf area index earth system data record from multiple sensors. Part 1: Theory, *Remote Sensing of Environment* (2008), doi:10.1016/j.rse.2008.07.014

In the above formulation, Terra MODIS LAI and FPAR products serve as the benchmark. It should be noted that the above technique falls into the category of the "probability approach to ill-posed problems" which is close to the decoding problem of information theory (Lavrentiev, 1967, pp. 8–9). It therefore naturally incorporates the notions "uncertainty" and "information".

3. Parameterization of canopy spectral reflectance

Retrievals of the LAI/FPAR ESDR from multiple sensors require parameterization of the retrieval algorithm that can be adjusted for the specific features of the Bidirectional Reflectance Factor (BRF) measurements by a particular sensor (spatial resolution, bandwidth, calibration, atmospheric correction, information content, etc., cf. Section 1). The radiative transfer theory of canopy spectral invariants provides the required BRF parameterization via a small set of well-defined measurable variables that specify the relationship between the spectral response of vegetation canopy bounded below by a non-reflecting surface to the incident radiation at the leaf and canopy scales (Wang et al., 2003; Huang et al., 2007; Lewis & Disney, 2007; Smolander & Stenberg, 2005).

3.1. Canopy spectral invariants

Photons that have entered the vegetation canopy undergo several interactions with leaves before either being absorbed or exiting the medium through its upper or lower boundary (Fig. 1). Interacting photons can either be scattered or absorbed by a phytoelement. The probability of a scattering event, or leaf single scattering albedo, ω_λ, depends on the wavelength and is a function of the leaf biochemical constitution. If objects are large compared to the wavelength of the radiation, e.g., leaves, branches, etc., the photon free path between two successive interactions is independent of the wavelength. The interaction probabilities for photons in a vegetation media, therefore, are determined by the structure of the canopy rather than photon frequency or the optical properties of the canopy. To quantify this feature, Smolander and Stenberg (2005) introduced the notion of recollision probability, p, defined as the probability that a photon scattered by a foliage element in the canopy will interact within the canopy again. This spectrally invariant parameter is a function of canopy structural arrangement only (Huang et al., 2007; Lewis & Disney, 2007). Scattered photons can escape the vegetation canopy either through the upper or lower boundary. Their angular distribution at the upper boundary is given by the directional escape probability, $\rho(\Omega)$ (Huang et al., 2007). Given recollision, p_m, and escape, $\rho_m(\Omega)$, probabilities as a function of scattering order, m, the bidirectional reflectance factor, $\mathrm{BRF}_{\mathrm{BS},\lambda}(\Omega)$, for a vegetation canopy bounded below by a non-reflecting surface can be expanded in a series of successive orders of scattering (Huang et al., 2007).

$$\mathrm{BRF}_{\mathrm{BS},\lambda}(\Omega) = \rho_1(\Omega)\omega_\lambda i_0 + \rho_2(\Omega)\omega_\lambda^2 p_1 i_0 + \cdots + \rho_m(\Omega)\omega_\lambda^m (p_1 p_2 \cdots p_{m-1}) i_0 + \cdots. \quad (1)$$

Here i_0 is the probability of initial collision, or canopy interceptance, defined as the proportion of photons from the incident beam that are intercepted, i.e., collide with foliage elements for the first time. This parameter gives the proportion of shaded area on the ground which in turn is directly related to the proportion of the sunlit leaf area. Canopy interceptance does not depend on the wavelength and is a function of the direction of the incident beam and canopy structure.

In the general case, the recollision and escape probabilities vary with the scattering order m. For $m=1$, the directional escape probability coincides with the bi-directional gap probability. These probabilities, however, reach plateaus as the number of interactions m increases. Monte Carlo simulations of the radiation regime in 3D canopies suggest that the probabilities saturate after 2 to 3 interactions for low to moderate LAI canopies (Lewis & Disney, 2007) with the recollision probability exhibiting a much faster convergence (Huang et al., 2007). Neglecting variations in p_m with m (i.e., $p_m \approx \mathrm{const} = p$) and in $\rho_m(\Omega)$ for $m>1$ (i.e., $\rho_m(\Omega) \approx \mathrm{const} = \rho_2(\Omega)$ for $m \geq 2$) in Eq. (1), one obtains the first order approximation for the $\mathrm{BRF}_{\mathrm{BS},\lambda}$ (Huang et al., 2007)

$$\mathrm{BRF}_{\mathrm{BS},\lambda}(\Omega) = \omega_\lambda R_1(\Omega) + \frac{\omega_\lambda^2}{1-p\omega_\lambda} R_2(\Omega). \quad (2)$$

Here $R_1(\Omega) = \rho_1(\Omega) i_0$ and $R_2(\Omega) = \rho_2(\Omega) p i_0$ are the escape probabilities expressed relative to the number of incident photons. The accuracy of this first order approximation depends on the difference between successive approximation to p multiplied by the factor $(\omega_\lambda p)^2/(1-\omega_\lambda p)$ (Huang et al., 2007).

Under the above assumption regarding dependence of the recollision probability on the scattering order, the spectral absorptance, $a_{\mathrm{BS},\lambda}$ of the vegetation canopy with non-reflecting background can be expressed as (Fig. 1)

$$a_{\mathrm{BS},\lambda} = \frac{1-\omega_\lambda}{1-p\omega_\lambda} i_0. \quad (3)$$

The corresponding FPAR is a weighted integral of Eq. (3) over the PAR spectral region (Knyazikhin et al., 1998a). According to Smolander and Stenberg (2005) Eq. (3) provides an accurate estimate of canopy spectral absorptance. A detailed analysis of the approximations given by Eqs. (2) and (3), their accuracies as well as how the recollision probability and canopy interceptance can be accurately measured in the field are discussed in Huang et al. (2007).

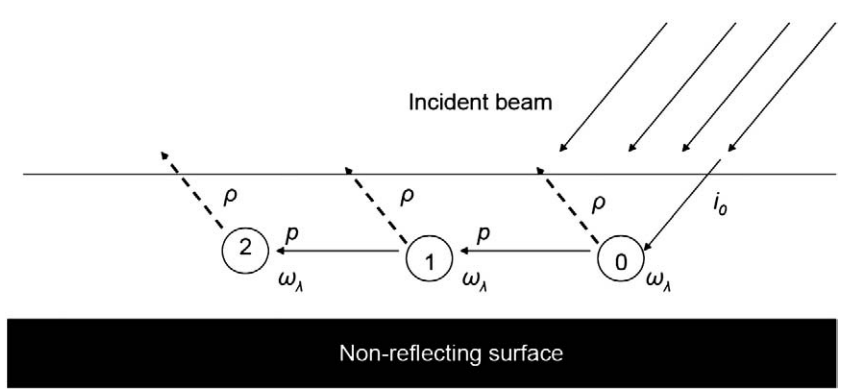

Fig. 1. Schematic plot of the photon-canopy interactions. Photons incident on the vegetation canopy will be intercepted by phytoelements with probability i_0. This probability of initial collision, or canopy interceptance, does not depend on wavelength and is a function of the direction of incident beam and canopy structure. The intercepted photons will be scattered by the foliage elements with probability ω_λ, and, in turn, will either interact again or escape the canopy with probabilities p and ρ, respectively. Given p_m and ρ_m as a function of scattering order m, the probability that photons from the incident beam will escape the vegetation after m interactions is $\rho_m \omega_\lambda^m (p_1 p_2 \cdots p_{m-1}) i_0$. The probability of absorption after m interactions is $(1-\omega_\lambda)\omega_\lambda^m (p_1 p_2 \cdots p_{m-1}) i_0$. The proportion of absorbed or exiting photons is equal to the sum of corresponding probabilities for scattering order m.

Please cite this article as: Ganguly, S., et al., Generating vegetation leaf area index earth system data record from multiple sensors. Part 1: Theory, *Remote Sensing of Environment* (2008), doi:10.1016/j.rse.2008.07.014

3.2. Canopy-ground interactions

The three-dimensional radiative transfer problem with arbitrary boundary conditions can be expressed as a superposition of some basic radiative transfer sub-problems with purely absorbing boundaries and to which the notion of spectral invariant can be directly applied (Knyazikhin & Marshak, 2000). These two problems are: (1) the black soil problem, "BS-problem", specified by the original illumination conditions at the top of the canopy and a completely absorbing soil at the bottom; (2) the soil problem, "S-problem", specified by no input energy at the top, but Lambertian energy sources at the bottom. This decomposition technique was implemented in the MODIS LAI/FPAR operational algorithm (Knyazikhin et al., 1998a). According to this approach, the spectral BRF and canopy spectral absorptance are approximated as

$$\mathrm{BRF}_\lambda(\Omega) = \mathrm{BRF}_{\mathrm{BS},\lambda}(\Omega) + \frac{\rho_{\mathrm{sur},\lambda}}{1-\rho_{\mathrm{sur},\lambda} r_{S,\lambda}} t_{\mathrm{BS},\lambda} J_{S,\lambda}(\Omega), \tag{4}$$

$$a_\lambda = a_{\mathrm{BS},\lambda} + \frac{\rho_{\mathrm{sur},\lambda}}{1-\rho_{\mathrm{sur},\lambda} r_{S,\lambda}} t_{\mathrm{BS},\lambda} a_{S,\lambda}. \tag{5}$$

The second term on the right hand side of Eqs. (4) and (5) describes the contribution to the BRF and absorptance from multiple interactions between the ground and vegetation (cf. Appendix). Here, $\rho_{\mathrm{sur},\lambda}$ is an effective ground reflectance, and $t_{\mathrm{BS},\lambda}$ is the transmittance of the vegetation canopy for the BS-problem. Variables $r_{S,\lambda}$, $a_{S,\lambda}$, and $J_{S,\lambda}(\Omega)$ represent solutions to the "S-problem". The expansion in successive order of scattering as given by Eq. (1) and illustrated in Fig. 1 is also applicable to the "S-problem", with the only difference that i_0 is replaced with $i_{0,S}$, the proportion of photons from sources below the canopy that are intercepted (i.e., those that collide with foliage elements for the first time). A full set of equations describing canopy-ground interaction is given in the Appendix.

Thus, a small set of well defined measurable variables provide an accurate parameterization of canopy optical and structural properties required to fully describe the spectral response of a vegetation canopy to incident solar radiation. This set includes spectrally varying soil reflectance ($\rho_{\mathrm{sur},\lambda}$), single-scattering albedo (ω_λ), spectrally invariant canopy interceptances (i_0 and $i_{0,S}$), recollision probability (p) and the directional escape probability (ρ_1 and ρ_2) and their hemispherically averaged values.

3.3. Generation of structural parameters

The global classification of canopy structural types utilized in the Collection 5 MODIS LAI/FPAR algorithm was adopted in this study (Shabanov et al., 2005; Yang et al., 2006). According to this classification, global vegetation is stratified into eight canopy architectural types or biomes: (1) grasses and cereal crops, (2) shrubs, (3) broadleaf crops, (4) savannas, (5) evergreen broadleaf forests, (6) deciduous broadleaf forests, (7) evergreen needle leaf forests and (8) deciduous needle leaf forests. The structural attributes of these biomes are parameterized in terms of variables that the transport theory admits (Knyazikhin et al., 1998a). The stochastic radiative transfer equation was used to generate the Collection 5 Look-up-Tables (LUT) — a set of tabulated BRF values as a function of biome type, LAI, view/illumination geometry, etc. (Shabanov et al., 2000; Huang et al., 2008). According to our strategy we first generate the spectrally invariant parameters for which the spectral BRF and absorptance coincide with corresponding entries of the Collection 5 MODIS LUTs for all combinations of LUT entries. Next, given these parameters, the BRF and absorptance for specific wavelengths can be calculated using Eqs. (2)–(5) and (A2)–(A4) with varying single scattering albedo which is used as the tuning parameter to adjust the LUTs for data spatial resolution and spectral band characteristics (cf. Sections 4 and 5).

The canopy interceptances can be directly calculated using the stochastic radiative transfer equation. Fig. 2 shows i_0 and $i_{0,S}$ as a function of LAI for one example vegetation type (savannas). Isotropic diffuse sources below the canopy are used to specify the interceptance $i_{0,S}$. Notably, $i_{0,S}$ is greater than i_0, that is, interception is higher under

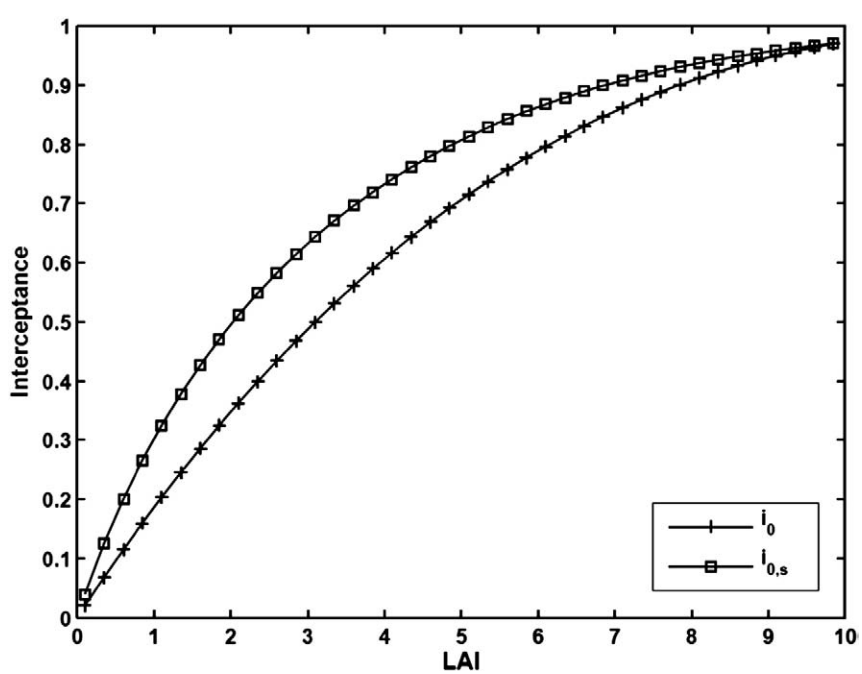

Fig. 2. Canopy interceptances i_0 and $i_{0,S}$ as a function of LAI. The latter is the proportion of photons from isotropic sources below the canopy that is intercepted by the vegetation. Calculations were performed for a vegetation canopy consisting of identical cylindrical "trees" uniformly distributed in the canopy layer bounded from below by both a non-reflecting (black soil problem) and reflecting (soil problem) surface. The canopy structure is parameterized in terms of the leaf area index of an individual tree, L_o, ground cover, g, crown height, H, and crown diameter D. The LAI varies with the ground cover as LAI=gL_o. The stochastic radiative transfer equation was used to derive canopy spectral interaction coefficient $i(\lambda)$ for both reflecting and non-reflecting surfaces. The interceptances i_0 and $i_{0,S}$ are obtained by fitting the spectral invariant approximation to $i(\lambda)$. The crown diameter, height and plant LAI are set to 1(in relative units), 2 and 10, respectively. The solar zenith angle and azimuth of the incident beam are 30° and 0°. The view zenith angle is nadir.

Please cite this article as: Ganguly, S., et al., Generating vegetation leaf area index earth system data record from multiple sensors. Part 1: Theory, *Remote Sensing of Environment* (2008), doi:10.1016/j.rse.2008.07.014

ARTICLE IN PRESS

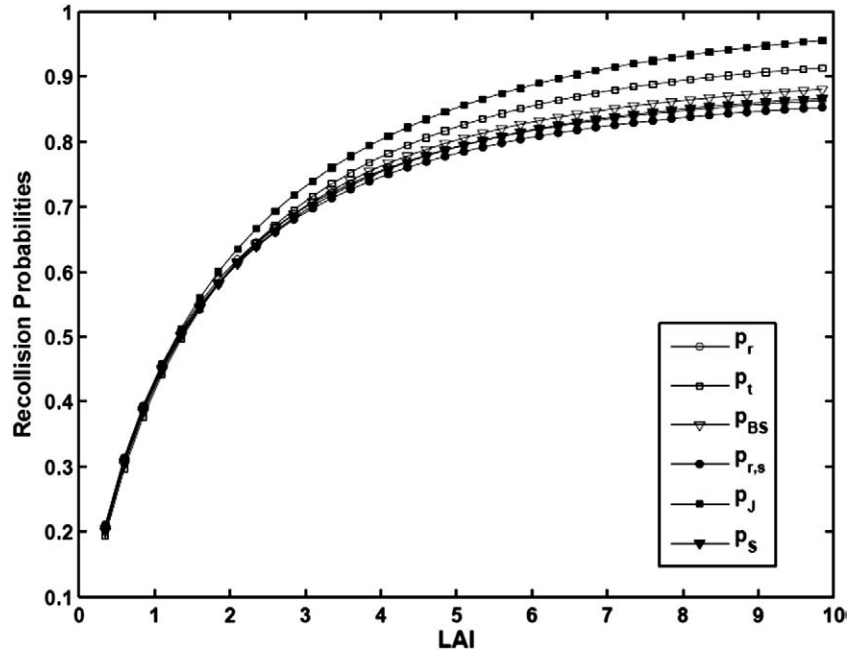

Fig. 3. Recollision probabilities calculated by fitting equations for the black soil (BRF_{BS}, a_{BS} and t_{BS}) and "S" (a_S, r_S, and t_S) problems to their simulated values. Here p_{BS} and p_S are specified by fitting a_{BS} and a_S; p_t and p_S by fitting t_{BS} and t_S; p_r and p_{rs} by fitting BRF_{BS} and r_S. Calculations were performed for the 3D vegetation canopy described in Fig. 2. The crown height, diameter and plant LAI are set to 1(in relative units), 2 and 10, respectively. The solar zenith angle and azimuth of the incident beam are 30° and 0°. The view zenith angle is nadir.

diffuse illumination conditions (Min, 2005; Gu et al., 2002), which is captured by our simulations.

The stochastic radiative transfer equation is used to simulate the solutions of the "BS-problem" (BRF_{BS}, a_{BS} and t_{BS}) and "S-problem" (a_S, r_S, and t_S) as a function of the single scattering albedo, ω, for various LAI and sun-view geometries. For given LAI and sun-view geometry, the spectrally invariant parameters are obtained by fitting the analytical approximations (cf. Eqs. (2), (3) and Appendix) to their simulated counterparts. The parameters thus obtained are functions of LAI and sun-view geometry. Fig. 3 shows the recollision probabilities calculated by fitting solutions for the "BS-problem" and "S-problem" to their simulated values. As expected, these variables are close to each other (Huang et al., 2007).

Given spectrally invariant parameters, the reflectances (r_{BS} and r_S), transmittances (t_{BS} and t_S), and absorptances (a_{BS} and a_S) are calculated for varying LAI and single scattering albedo values using the spectral invariant approximations and checked for validity of the energy conservation law, $r+t+a=1$, for both the "BS-" and "S-" problems (Fig. 4). Note that the accuracy of $r+t+a=1$ follows the accuracy of the first order approximation given by the factor $(\omega_\lambda p)^2/(1-\omega_\lambda p)$ (Section 3.1); that is,

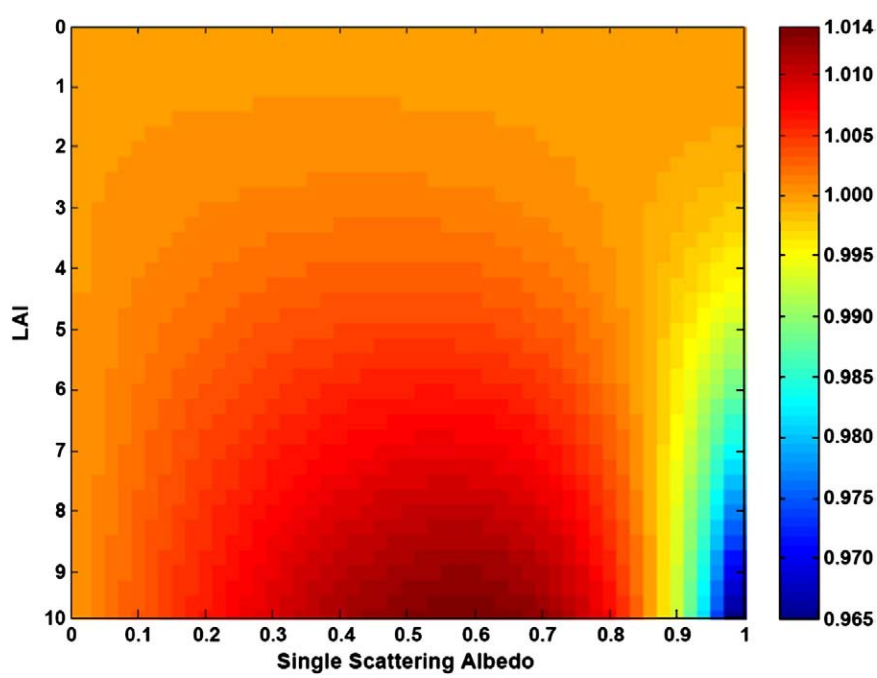

Fig. 4. Values of the energy conservation relationships $r_{BS}+t_{BS}+a_{BS}$ as a function of single scattering albedo and LAI. Calculations were performed for the 3D vegetation canopy described in Fig. 2. Parameters r_{BS}, t_{BS} and a_{BS} are obtained from the spectral invariant approximation to the reflectance, transmittance and absorption values as derived from the stochastic radiative transfer simulations.

Please cite this article as: Ganguly, S., et al., Generating vegetation leaf area index earth system data record from multiple sensors. Part 1: Theory, *Remote Sensing of Environment* (2008), doi:10.1016/j.rse.2008.07.014

the closer p and ω_λ to 1, the lower the accuracy is. Finally, BRFs at red and NIR spectral bands corresponding to values of single scattering albedo of Collection 5 MODIS LUT are calculated as a function of the effective ground reflectances at red and NIR wavelengths, LAI and sun-view geometry. The BRF values are compared with corresponding values stored in the Collection 5 MODIS LUTs to ensure consistency (Fig. 5).

4. Algorithm adjustment for the sensors spatial resolution

Our scaling approach is based on the scale dependence of the single scattering albedo. This variable is defined as the probability that a photon intercepted by foliage elements in volume V will escape V. The volume V is associated with the scale at which the single scattering albedo is defined, e.g., single leaf, clump of leaves, tree crown, patch, or even a satellite pixel. The theory of canopy spectral invariants provides an accurate description of variations in the single scattering albedo with scale V (Smolander & Stenberg, 2005; Lewis & Disney, 2007). In our approach, BRF is an explicit function of the single scattering albedo and thus this theory can be applied to imbue scale dependence to the algorithm. The aim of this section is to demonstrate how the canopy spectral invariant relationships can be employed to adjust solutions of the "BS" and "S" problems for sensor resolutions.

Consider two volumes, V_0 and V, representing pixel and tree crown scales. Their single scattering albedos $\omega_\lambda(V_0)$ and $\omega_\lambda(V)$ quantify the scattering properties of the pixel V_0 and its constituent objects of volume V. The latter are distributed within V_0 in a certain fashion. It follows from Eq. (3) that the pixel single scattering albedo, $\omega_\lambda(V_0)$, can be estimated as (Smolander & Stenberg, 2005; Lewis & Disney, 2007)

$$\omega_\lambda(V_0) = \frac{i_0(V_0) - a_{bs,\lambda}(V_0)}{i_0(V_0)} = \omega_\lambda(V)\frac{1-p(V\to V_0)}{1-\omega_\lambda(V)p(V\to V_0)}. \quad (6)$$

Here $i_0(V_0)$ is the proportion of photons intercepted by the volume V_0 (Fig. 1), and $p(V\to V_0)$ is the recollision probability, defined as the probability that a photon scattered by volume V (e.g., by a tree crown) resident in the pixel V_0 will hit another volume V (e.g., another tree crown) in the same pixel. Its value is determined by the distribution of volumes V (e.g., tree crowns) within V_0.

Eq. (6) links canopy spectral behavior at the pixel and tree crown scales. Indeed, the canopy single scattering albedo $\omega_\lambda(V_0)$ (pixel scale) is an explicit function of the spectrally varying single scattering albedo $\omega_\lambda(V)$ at the tree crown scale V and the spectrally invariant recollision probability $p(V\to V_0)$. The latter is a scaling parameter that accounts for the cumulative effect of canopy structure from tree crown to pixel scales. Both $\omega_\lambda(V)$ and $p(V\to V_0)$ vary with scale V. For example, the single scattering albedo and the recollision probability associated with needle, shoot, branch, tree crown, etc., are different (Smolander & Stenberg, 2003). However since the left-hand side of Eq. (6) does not depend on V, the algebraic expression on the right-hand side of this equation should also be independent of the scale V. Based on this property, Smolander and Stenberg (2005) specified variation in the leaf single scattering albedo and the recollision probability with the scale V as follows.

Consider the scale V (e.g., tree crown) which in turn consists of smaller objects (e.g. clump of leaves) distributed in V. Let V' and $\omega_\lambda(V')$ represent the scale of the object and its single scattering albedo. Eq. (6) can also be applied to the volume V, i.e.,

$$\omega_\lambda(V) = \omega_\lambda(V')\frac{1-p(V'\to V)}{1-\omega_\lambda(V')p(V'\to V)}. \quad (7)$$

Substitution of this equation into Eq. (6) results in the same equation for $\omega_\lambda(V_0)$ with the only difference that $\omega_\lambda(V)$ is replaced with $\omega_\lambda(V')$ and $p(V\to V_0)$ is replaced with a new recollision probability $p(V'\to V_0)$ calculated as

$$p(V'\to V_0) = p(V'\to V) + [1-p(V'\to V)]p(V\to V_0). \quad (8)$$

One can see the probability $p(V'\to V_0)$ that a photon scattered by a volume V' (e.g., clump of leaves) will interact within the pixel V_0 again follows the Bayes' formula given by Eq. (8). The recollision probability, therefore, is a scaling parameter that accounts for the cumulative effect of multi-level hierarchical structure in a vegetated pixel.

Smolander and Stenberg (2003, 2005) demonstrated the validity of the scaling relationships for needle (V' = needle) and shoot (V' = shoot) scales. Lewis and Disney (2007) found that Eqs. (6)–(8) are applicable to the within leaf (V' = a within-leaf scattering object) and leaf (V' = leaf) scales, implying that scaling equations provide a framework through which structural information can be maintained in a consistent manner across multiple scales from within-leaf to canopy level scattering. Tian et al. (2002) used a semi-empirical approach to account for biome mixtures within a coarse resolution pixel.

The scaling properties of the scattering process underlie our approach for developing scale-dependent formulation of the radiative transfer process in vegetation canopies. First, one defines a base scale, V, in a canopy-radiation model, e.g., tree crown, patch, etc. The structure-dependent coefficients that appear in the radiative transfer equation are parameterized in terms of the distribution of objects in the volume V within the pixel V_0 and thus are independent of the structure that exists within V. The concepts of the pair-correlation function (Huang et al., 2008) and biome mixtures (Shabanov et al., 2007) are used to obtain these coefficients. Second, the single scattering albedo $\omega_\lambda(V)$ of the object (which also appears in the equation) is calculated using Eqs. (7) and (8). The radiative transfer equation describes the interaction between photons and objects of the volume V while multiple scattering within V is accounted by the single scattering albedo $\omega_\lambda(V)$.

In our parameterization (cf. Section 3), canopy reflectance and absorptance are explicit functions of structural parameters and single scattering albedo. The accuracy of the approximation depends on $[\omega_\lambda(V)p(V\to V_0)]^2/[1-\omega_\lambda(V)p(V\to V_0)]$; that is, the smaller the p value, the more accurate the approximation is (Huang et al., 2007). It follows from Eqs. (7) and (8) that the single scattering albedo and the recollision probability are decreasing functions of V, i.e., $\omega_\lambda(V)\le\omega_\lambda(V')$ and $p(V\to V_0)\le p(V'\to V_0)$ if $V'\subset V$. In other words, the smaller the base scale, the more hierarchical levels of the vegetation in a pixel are involved, and more accurately the contributions of scattering orders should be accounted to estimate canopy absorptive and reflective

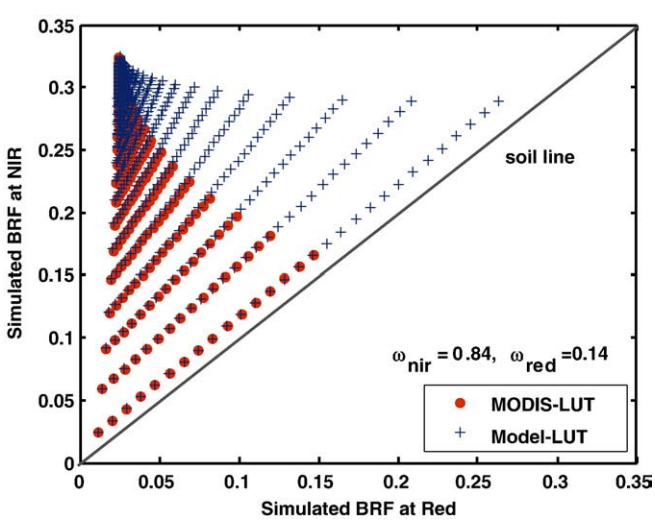

Fig. 5. The spectral invariant approximation to the BRF superimposed on the MODIS LUTs entries for the BRF. The effective ground reflectance patterns for the MODIS LUT are restricted to dark and intermediate brightnesses for illustration purpose, while the spectral invariant simulation includes backgrounds ranging from dark to bright soils. The red-NIR spectral space is displayed for the broadleaf forest vegetation class, characterized by the single scattering albedos at the NIR(ω_{nir}=0.84) and red (ω_{red}=0.14) bands. Calculations were performed for the 3D vegetation canopy described in Fig. 2. The solar zenith angle and azimuth of the incident beam are 30° and 0°. The view zenith angle is nadir.

properties (Knyazikhin et al., 1998b). The base scale therefore should be chosen sufficiently large to minimize the number of hierarchical levels and to achieve a good accuracy in the first order approximation.

In our approach, the structural variables are calculated for a homogeneous pixel of a single vegetation type only. The base scale represents an individual plant (e.g., tree in a woody vegetation class) or a group of plants (e.g., in grasses). When the spatial resolution of the imagery decreases (i.e., the volume V_0 increases), the degree of vegetation mixing within the pixel increases. It means that different structures can exist at the base scale and consequently more hierarchical levels of the canopy structure may be present in the imagery. This directly follows from Eq. (8), i.e., $p(V' \to V_0) \geq p(V' \to V)$ if $V_0 \supset V$. Assuming $p(V \to V_0)$ varies continuously with the base scale V and the resolution V_0, an increase in the recollision probability due to increase in V_0 can be compensated by an increase in V such that $p(V, V_0) = p(\overline{V}, \overline{V}_0)$ where $\overline{V} \supset V$ and $\overline{V} \supset V_0$. Thus, the structural parameters can be pre-calculated for a fixed base scale. The spectral $\mathrm{BRF}_{\mathrm{BS},\lambda}$ (and solutions to the "S" problem) can be adjusted for the resolution by using the single scattering albedo $\omega_\lambda(V)$ at a scale V. The single scattering albedo therefore allows us to scale up the simulated BRF to a coarser resolution.

5. Algorithm adjustment for the sensors spectral bandwidth

For a given spectral band, the observed BRF is a weighted integral of the spectral BRF over a spectral interval, i.e., the bandwidth. The weight is the spectral response function that describes the sensitivity of the sensor to a particular wavelength in the spectral interval. Both the weight and the interval are sensor specific and vary with the spectral band. Fig. 6 shows spectral response functions for red (580 nm $\leq \lambda \leq$ 680) and NIR (725 nm $\leq \lambda \leq$ 1100) spectral bands for the NOAA 16 AVHRR sensor (WWW1). The corresponding MODIS spectral bands, 620 nm $\leq \lambda \leq$ 670 nm and 841 nm $\leq \lambda \leq$ 876, are much narrower and shapes of the response functions (WWW2) differ from their AVHHR counterparts (Fig. 6). The difference in the spectral band characteristics is a factor that changes spectral signatures of pixels measured by two sensors. In our parameterization, the structural and radiometric components of the measured signal are separated. This feature gives us a simple way to adjust the algorithm for sensor band characteristics. Since the solution of the "BS-problem" is a major source of information about the intrinsic canopy properties, we focus on this component of the signal.

The measured reflectance, $\mathrm{BRF}_{\mathrm{M},\lambda}$, is a weighted integral of Eq. (2) over a spectral interval $\alpha \leq \lambda \leq \beta$, i.e.,

$$\mathrm{BRF}_{\mathrm{M},\lambda}(\Omega) = R_1(\Omega)\,\bar{\omega}_\lambda + \gamma(p)\frac{\bar{\omega}_\lambda^2}{1-p\,\bar{\omega}_\lambda}R_2(\Omega). \tag{9}$$

Here $\bar{\omega}_\lambda = \int_\alpha^\beta \omega_\lambda f(\lambda)d\lambda$ is the mean single scattering albedo; $f(\lambda)$, $\int_\alpha^\beta f(\lambda)d\lambda = 1$, is the spectral response function, and

$$\gamma(p) = \left(\int_\alpha^\beta \frac{\omega_\lambda^2}{1-p\omega_\lambda}f(\lambda)d\lambda\right)\left(\frac{\bar{\omega}_\lambda^2}{1-p\,\bar{\omega}_\lambda}\right)^{-1}. \tag{10}$$

Note that $\omega_\lambda^2/(1-p\omega_\lambda)$ in the integral term of Eq. (10) is a convex function with respect to values of the single scattering albedo. It follows from the Jensen's inequality (Gradshteyn & Ryzhik, 1980) for convex functions that the numerator in Eq. (10) is no less than the denominator, and thus, $\gamma(p) \geq 1$.

Values of ω_λ and $\gamma(p)$ depend on the variation of the single scattering albedo ω_λ with wavelength. If the single scattering albedo is constant in the interval $\alpha \leq \lambda \leq \beta$, then $\omega_\lambda = \omega_\lambda$ and $\gamma(p) = 1$ and no adjustment is needed. Such a situation is typical for NIR spectral bands in which the single scattering albedo is almost flat with respect to wavelength. The single scattering albedo exhibits much stronger variation at wavelengths between 580 nm and 680 nm. In this interval, ω_λ is a decreasing function with a local minimum at about 680 nm. The averaging of ω_λ over the red AVHHR spectral band results in a higher value of ω_λ than over the narrower spectral interval of the red MODIS band. This effect tends to increase the measured AVHRR surface reflectances at red compared to the corresponding MODIS values.

The variation of ω_λ causes the ratio $\gamma(p)$ to deviate from unity which enhances the measured reflectance. Fig. 7 shows $\gamma(p)$ for red and NIR spectral bands for AVHRR and MODIS. The ratio is an increasing function with respect to the recollision probability. For the NIR spectral band, $\gamma(p)$ is very close to unity, with maximum deviation being less than 0.5%. For the red spectral band, values of the ratio are higher and can deviate from unity by 8%. However, the overall variation in the ratio does not exceed 2%. In this example, the ratio was calculated using a typical single scattering albedo of an individual leaf and thus its values correspond to the leaf scale. Recall that the single scattering albedo and the recollision probability are decreasing functions of the base scale. It follows from Eq. (10) that the change in the single scattering albedo by a factor k alters the ratio from $\gamma(p)$ to

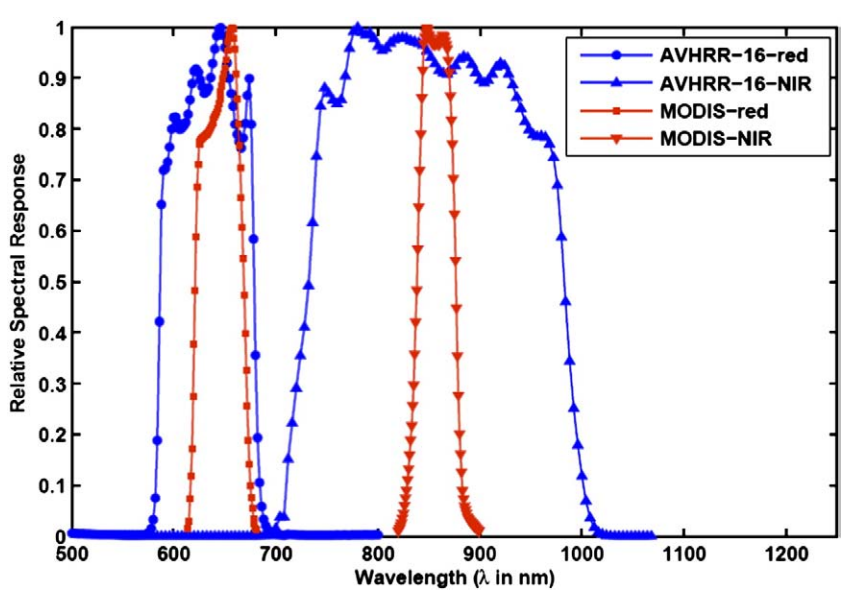

Fig. 6. Relative spectral response function in the red and NIR spectral intervals for the NOAA AVHRR-16 and MODIS sensors.

Please cite this article as: Ganguly, S., et al., Generating vegetation leaf area index earth system data record from multiple sensors. Part 1: Theory, *Remote Sensing of Environment* (2008), doi:10.1016/j.rse.2008.07.014

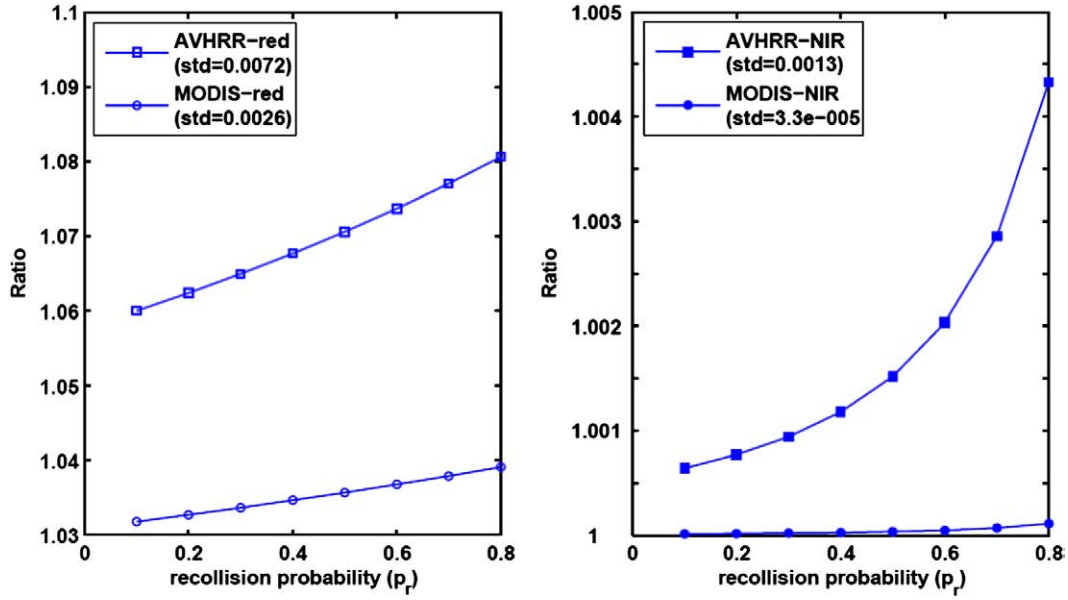

Fig. 7. The ratio $\gamma(p)$ for red and NIR spectral bands for AVHRR and MODIS. Spectral response functions shown in Fig. 6 for AVHRR-16 and MODIS and mean single scattering albedo of spruce needles (Huang et al., 2007) are used to calculate the ratio ("std" in the figure refers to standard deviation of $\gamma(p)$).

$\gamma(k{\cdot}p)$. The adjustment of the reflectance for a coarser data resolution, therefore, lowers its variation due to decreases in both the single scattering albedo ($k \leq 1$) and the recollision probability.

To summarize, the problem of accounting for differences in spectral characteristics between sensors can be reduced to finding band dependent values of the single scattering albedo that compensate for changes in ω_λ due to differences in the bandwidths and deviation of $\gamma(p)$ from unity due to variation in ω_λ, where the latter is dependent on the base scale. The single scattering albedo therefore is the basic configurable parameter to adjust the simulated MODIS BRF for the spatial resolution and spectral band composition of the AVHRR sensor. Its value can be specified by fitting the simulated BRF to the observed BRF values over different vegetation types during the green peak season (Hu et al., 2003; Shabanov et al., 2005). This technique will be demonstrated in the second paper of this series.

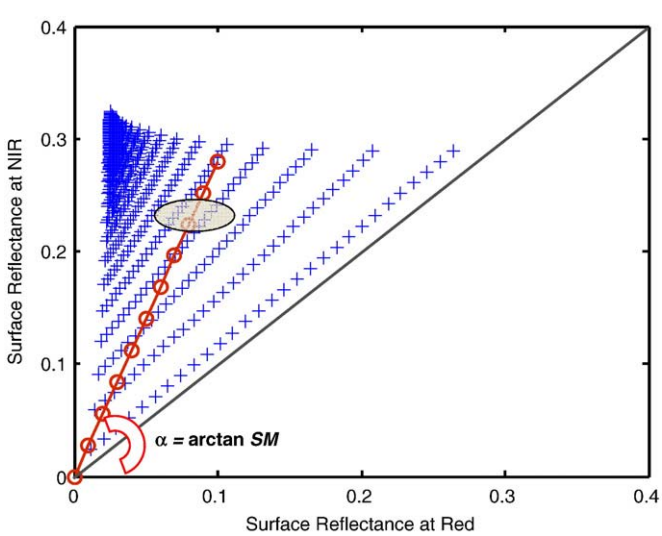

Fig. 8. Reflectance of vegetated surface in the red-NIR spectral plane. The cross symbols mark the spectral space of the MODIS LAI/FPAR LUTs for a range of simulated LAI and soil background brightnesses. The line with circles intersects the origin at an angle defining the Simple Ratio. This line depicts different possible combinations of red and near-infrared reflectances corresponding to different LAI values and soil spectral reflectance patterns. The ellipse represents the inequality criterion for which the solution set is obtained.

6. Data information content and observation uncertainty

The difference in information content of MODIS surface reflectance and AVHRR NDVI can be quantified as follows. The spectral reflectance of a surface can be depicted as a point in the red-NIR spectral space. The location of the point in the polar coordinate system is given by the polar angle, $\alpha = \tan^{-1}(\mathrm{NIR}/\mathrm{RED}) = \tan^{-1}(\mathrm{SM})$, and the radius $r = \sqrt{\mathrm{NIR}^2 + \mathrm{RED}^2}$. Here RED and NIR represent BRF values at red and NIR spectral bands. Pixels with the same NDVI are located on a straight line (red line in Fig. 8). This line intersects the origin of the spectral plane at an angle α. In the case of MODIS, the surface reflectance data provide both the angle and location on the line, while the AVHRR NDVI data provide the angle only.

The MODIS LAI/FPAR algorithm exploits the location information by attributing each point in the spectral space to a specific physical state that is characterized by a background brightness and LAI. A pixel

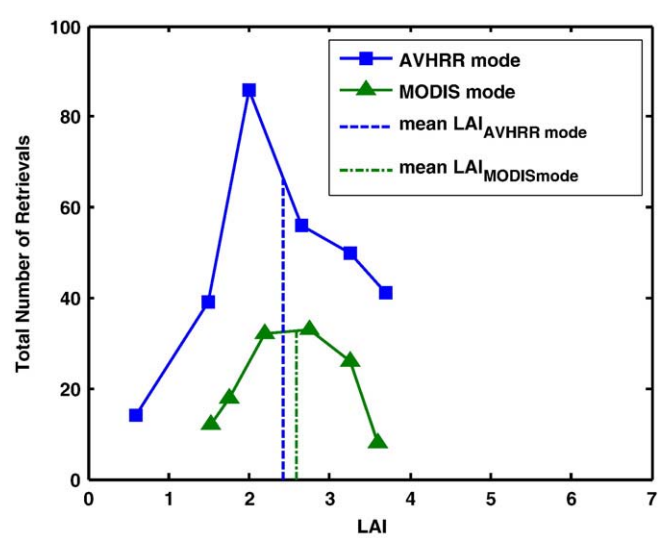

Fig. 9. Distribution of acceptable LAI values corresponding to the full range of possible values of the radius (squares) and to a specific value of the radius (triangles). The mean LAI values and their dispersions are taken as the LAI retrievals and their uncertainties. The AVHHR and MODIS modes were applied to the MODIS surface reflectance using the MODIS LUT.

Please cite this article as: Ganguly, S., et al., Generating vegetation leaf area index earth system data record from multiple sensors. Part 1: Theory, *Remote Sensing of Environment* (2008), doi:10.1016/j.rse.2008.07.014

can have a background ranging from dark to bright soils, and the LAI can vary over a range for each specific instance of background brightness. In order to meet consistency requirements formulated in Section 2, we implemented a specific mode in the MODIS algorithm ("AVHRR mode"), in which the angle, α, and a range ($r_{min} \le r \le r_{max}$) of valid radii are taken as inputs. This range corresponds to variations of r for given α as given by Collection 5 MODIS LUTs. While executing the algorithm in the AVHRR mode, the following situations are possible (cf. Fig. 8):

- If $r_{min}=r_{max}$, the set of acceptable solutions coincides with that generated by the operational MODIS LAI/FPAR algorithm.
- If $r_{min}<r_{max}$, the set of acceptable solutions includes as subset standard MODIS retrievals (Fig. 9).

The following merit function is used to select the set of acceptable solutions in the MODIS-algorithm,

$$\Delta^2 = \frac{\left(\mathrm{NIR}^* - \mathrm{NIR}\right)^2}{\sigma_{\mathrm{NIR}}^2} + \frac{\left(\mathrm{RED}^* - \mathrm{RED}\right)^2}{\sigma_{\mathrm{RED}}^2}. \tag{11}$$

Here NIR^* and RED^* denote values of measured surface reflectances, while NIR and RED correspond to values of simulated reflectances. The dispersions σ_{NIR} and σ_{RED} quantify combined model and observations uncertainties at NIR and red spectral bands and are configurable parameters in our approach (Wang et al., 2001). The dispersions are represented as, $\sigma_{\mathrm{NIR}}=\varepsilon_{\mathrm{NIR}}\cdot\mathrm{NIR}^*$ and $\sigma_{\mathrm{RED}}=\varepsilon_{\mathrm{RED}}\cdot\mathrm{RED}^*$, where $\varepsilon_{\mathrm{NIR}}$ and $\varepsilon_{\mathrm{RED}}$ are the corresponding relative uncertainties (Wang et al., 2001). The variable Δ^2 characterizing the proximity of measured surface reflectances to simulated values has a chi-square distribution with two degrees of freedom. A value of $\Delta^2 \le 2$ indicates good proximity between observations and simulations (Wang et al., 2001). All LAI and soil reflectance values satisfying this criterion constitute the set of acceptable solutions for a particular MODIS observation (NIR^* and RED^*).

In the AVHRR-mode, the criteria $\Delta^2 \le 2$ is applied to each point on the line (Fig. 8), i.e., for $\mathrm{NIR}^* = r \cdot \sin\alpha = r \cdot \mathrm{SM}^* / \sqrt{1+\mathrm{SM}^{*2}}$, and $\mathrm{RED}^* = r \cdot \cos\alpha = r / \sqrt{1+\mathrm{SM}^{*2}}$. Here, SM^* is the input simple ratio from AVHRR, and the radius r varies between r_{min} and r_{max}. Note that the AVHRR mode does not increase computation time since in the MODIS mode the inequality $\Delta^2 \le 2$ is checked for all combinations of LAI and soil patterns.

Fig. 10 shows correlation between LAI retrievals using MODIS and AVHHR modes of the algorithm. In both modes, the algorithm generates similar mean LAI values given data from the same instrument. The corresponding dispersions, however, can differ significantly, indicating varying information content of retrievals. Recently, Hu et al. (2007) compared MODIS and MISR LAI seasonal profiles retrieved from data which have the same accuracy but different information content (Fig. 4 in the cited paper). The use of multi-angle and spectral information allows capturing seasonal LAI variations that are not detected by single-angle views. We will explore the impact of the information content on retrievals with respect to MODIS and AVHRR retrievals in the second paper of this series.

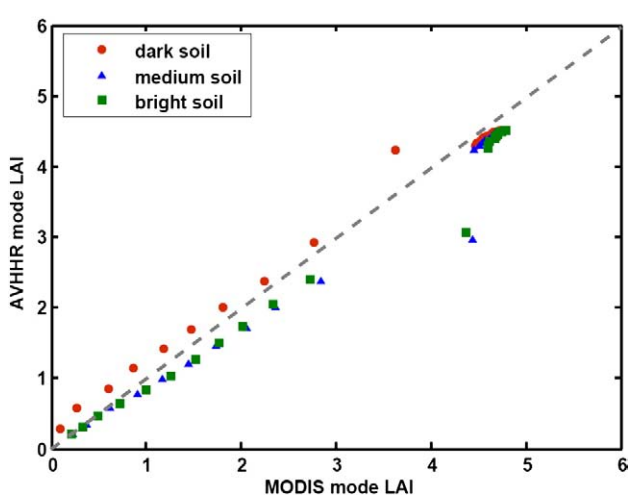

Fig. 10. Correlation between LAI values retrieved using the MODIS (horizontal axis) and AVHHR (vertical axis) modes of the algorithm for dark ($\rho_{sur,RED}=\rho_{sur,RED}=0.05$), medium ($\rho_{sur,RED}=\rho_{sur,RED}=0.16$) and bright ($\rho_{sur,RED}=\rho_{sur,RED}=0.26$) backgrounds. Surface reflectances shown in Fig. 8 that correspond to selected backgrounds and simple ratio (SM) calculated from the surface reflectances were used as input. The relative uncertainties at red and NIR spectral bands were set to 0.3 and 0.15.

7. Concluding remarks

This research introduces a physically based approach for generating LAI and FPAR ESDRs (this paper) and its application to developing a long time series of these products from MODIS and AVHRR data (second paper in this series). In general, ESDR algorithms ingesting data from different instruments should account for differences in spatial resolution, spectral characteristics, uncertainties due to atmospheric effects and calibration, information content, etc. Our approach to this problem is based on the radiative transfer theory of spectral invariants. Accordingly, the canopy spectral BRF is parameterized in terms of a compact set of parameters — spectrally varying soil reflectances, single-scattering albedo, spectrally invariant canopy interceptance, recollision probability and the directional escape probability. The approach ensures energy conservation and allows decoupling the structural and radiometric components of the BRF. According to this theory, the single scattering albedo accounts for the dependence of BRF on sensor's spatial resolution and spectral bandwidth. The parameter characterizing data uncertainty accounts for variation in the information content of the remote measurements. Thus, the single scattering albedo and data uncertainty are two key configurable parameters in our algorithm. The algorithm supports two modes of operation: the MODIS mode (retrievals from BRF) and the AVHRR mode (retrievals from NDVI). In both cases, the algorithm simulates similar mean LAI values, if input data from the same instrument are used. The corresponding dispersions, however, differ significantly, indicating varying input information content and related uncertainties (MODIS BRF vs. AVHRR NDVI). Overall, the problem of generating LAI/FPAR is reduced to the problem of finding values of data uncertainty and single scattering albedo for which: a) the consistency requirements for retrievals from MODIS and AVHRR are met; b) the difference between MODIS and AVHRR LAI/FPAR is minimized; c) the probability of retrieving LAI/FPAR is maximized. The implementation of this algorithm and evaluation of the derived product will be detailed in the second paper of this two-part series.

Acknowledgements

This research was funded by NASA Earth Science Enterprise. We thank Dr. C. J. Tucker of NASA GSFC for making the GIMMS NDVI data available.

Appendix A. Analytical expression of the "S" problem

The second term on the right hand side of Eqs. (4) and (5) describes the contribution of multiple interactions between the ground and the canopy to the total canopy BRF and absorptance. Let the downward flux at the surface level be $t_{BS,\lambda}$ in the case of a black surface. The incoming flux after interacting with the ground will act as the initial source at the surface. The reflected radiation flux ($t_{BS,\lambda}\ \rho_{sur,\lambda}$) will interact with the canopy further and return to the surface ($t_{BS,\lambda}\ \rho_{sur,\lambda}\ r_{S,\lambda}$), where $\rho_{sur,\lambda}$ and $r_{S,\lambda}$ are the hemispherically integrated ground and canopy reflectance, respectively. Let $J_{S,\lambda}(\Omega)$ be the radiance generated by isotropic sources ($1/\pi$) at the canopy bottom. Taking into account that the intensity of sources at the first interaction is

($\pi^{-1}t_{BS,\lambda}\ \rho_{sur,\lambda}$), the corresponding radiance from the surface can be expressed as ($J_{S,\lambda}(\Omega)\ t_{BS,\lambda}\ \rho_{sur,\lambda}$.). The total radiance, S, can be expressed as the sum of successive orders of scattering,

$$S = t_{BS,\lambda}\rho_{sur,\lambda}J_{S,\lambda}(\Omega) + \rho^2_{sur,\lambda}r_{S,\lambda}t_{BS,\lambda}J_{S,\lambda}(\Omega) + \rho^3_{sur,\lambda}r^2_{S,\lambda}t_{BS,\lambda}J_{S,\lambda}(\Omega) + \ldots + \rho^n_{sur,\lambda}r^{n-1}_{S,\lambda}t_{BS,\lambda}J_{S,\lambda}(\Omega),$$

where n is the order of scattering. The above geometric series can be rewritten in the closed form

$$S = \frac{\rho_{sur,\lambda}}{1-\rho_{sur,\lambda}r_{S,\lambda}}t_{BS,\lambda}J_{S,\lambda}(\Omega). \tag{A1}$$

The spectral invariant approximations for $t_{BS,\lambda}$ and $J_{S,\lambda}(\Omega)$ are

$$t_{BS,\lambda}(\Omega) = t_0 + \omega_\lambda T_1(\Omega) + \frac{\omega^2_\lambda T_2(\Omega)}{1-p_t\omega_\lambda}, \tag{A2}$$

$$J_{S,\lambda}(\Omega) = J_0 + \omega_\lambda J_1(\Omega) + \frac{\omega^2_\lambda J_2(\Omega)}{1-p_J\omega_\lambda}, \tag{A3}$$

where, the term t_0 is the zero order direct transmittance, $T_1(\Omega)=\tau_1(\Omega)i_0$ and $T_2(\Omega)=\tau_2(\Omega)p_t i_0$. τ_1 and τ_2 are probabilities that the scattered photons can escape the lower boundary of the canopy. $J_0, J_1(\Omega)$ and $J_2(\Omega)$ are analogous to t_0, $T_1(\Omega)$ and $T_2(\Omega)$. The term $t_{BS,\lambda}$ is the sum of the two components. The first is the zero order or uncollided transmittance, $t_0 = 1 - i_0$, which is defined as the probability that a photon in the incident flux will arrive at the bottom of canopy without suffering a collision. The second component represents transmittance of the diffuse radiation, i.e., the probability that a photon will exit the vegetation canopy through the lower boundary after one or more interactions. The expression for diffuse transmittance is obtained by hemispherically averaging Eq. (1) over downward directions. The expression for spectral reflectance, $r_{S,\lambda}$, is obtained by hemispherically integrating Eq. (1), formulated for $i_{0,S}$ instead of i_0, over the upper hemisphere,

$$r_{S,\lambda} = \omega_\lambda \bar{R}_{1,S} + \frac{\omega^2_\lambda \bar{R}_{2,S}}{1-p_{r,S}\omega_\lambda}. \tag{A4}$$

This equation can be used to approximate canopy reflectance in the case of the three-dimensional radiative transfer equation and non-Lambertian surface by parameterizing ground reflective properties in terms of an effective ground reflectance and anisotropy (Knyazikhin et al., 1998a). The latter is used as a source at the canopy bottom that generate the radiation field $J_{S,\lambda}$.

References

Baret, F., & Guyot, G. (1991). Potentials and limits of vegetation indices for LAI and APAR assessment. *Remote Sensing of Environment*, *35*, 161–173.

Chen, J. M., Pavlic, G., Brown, L., Cihlar, J., Leblanc, S. G., White, H. P., et al. (2002). Derivation and validation of Canada-wide coarse resolution leaf area index maps using high-resolution satellite imagery and ground measurements. *Remote Sensing of Environment*, *80*, 165–184.

Combal, B., Baret, F., Weiss, M., Trubuil, A., Mace, D., Pragnere, A., et al. (2002). Retrieval of canopy biophysical variables from bi-directional reflectance using prior information to solve the ill-posed problem. *Remote Sensing of Environment*, *84*(1), 1–15.

Committee on Earth Science and Applications from Space: A Community Assessment and Strategy for the Future (NRC Decadal Survey) (2007). *National Research Council, Earth Science and Applications from Space: National Imperatives for the Next Decade and Beyond*. 0-309-66900-6.

Choulli, M., & Stefanov, P. (1996). Reconstruction of the coefficient of the stationary transport equation from boundary measurements. *Inverse Problems*, *12*, L19–L23.

Demarty, J., Chevallier, F., Friend, A. D., Viovy, N., Piao, S., & Ciais, P. (2007). Assimilation of global MODIS leaf area index retrievals within a terrestrial biosphere model. *Geophysical Research Letters*, *34*, L15402. doi:10.1029/2007GL030014

Dickinson, R.E., Hendersen-Sellers, A., Kennedy, P.J., & Wilson, M.F. (1986). Biosphere-Atmosphere Transfer Scheme (BATS) for the NCAR CCM, NCAR Res., Boulder, CO, NCAR/TN-275-STR.

Diner, D. J., Asner, G. P., Davies, R., Knyazikhin, Y., Muller, J. P., Nolin, A. W., et al. (1999). New directions in Earth observing: scientific application of multi-angle remote sensing. *Bulletin of the American Meteorological Society*, *80*(11), 2209–2228.

Diner, D. J., Braswell, B. H., Davies, R., Gobron, N., Hu, J., Jin, Y., et al. (2005). The value of multiangle measurements for retrieving structurally and radiatively consistent properties of clouds, aerosols, and surfaces. *Remote Sensing of Environment*, *97*, 495–518.

GCOS (2006). Systematic observation requirements for satellite-based products for climate. WMO/TD No. 1338. September 2006 (2006) 103 pp. (available at http://www.wmo.ch/web/gcos/gcoshome.html).

Gobron, N., Pinty, B., Aussedat, O., Chen, J. M., Cohen, W. B., Fensholt, R., et al. (2006). Evaluation of fraction of absorbed photosynthetically active radiation products for different canopy radiation transfer regimes: methodology and results using Joint Research Center products derived from SeaWiFS against ground-based estimations. *Journal of Geophysical Research*, *111*, D13110. doi:10.1029/2005JD006511

Gradshteyn, I. S., & Ryzhik, I. M. (1980). *Table of Integrals, Series, and Products* (pp. 1160). New York: Academic Press.

Gu, L., Baldocchi, D., Verma, S. B., Black, T. A., Vesala, T., Falge, E. M., et al. (2002). Advantages of diffuse radiation for terrestrial ecosystem productivity. *Journal of Geophysical Research*, *107*, D6. doi:10.1029/2001JD001242

Gutman, G. G. (1998). On the use of long-term global data of land reflectances and vegetation indices derived from the advanced very high resolution radiometer. *Journal of Geophysical Research*, *104*, 6241–6256.

Hu, J., Tan, B., Shabanov, N. V., Crean, K. A., Martonchik, J. V., Diner, D. J., et al. (2003). Performance of the MISR LAI and FPAR algorithm: a case study in Africa. *Remote Sensing of Environment*, *88*, 324–340.

Hu, J., Su, Y., Tan, B., Huang, D., Yang, W., Bull, M. A., et al. (2007). Analysis of the MISR LAI/FPAR product for spatial and temporal coverage, accuracy and consistency. *Remote Sensing of Environment*, *107*, 334–347.

Huang, D., Knyazikhin, Y., Dickinson, R. E., Rautiainen, M., Stenberg, P., Disney, M., et al. (2007). Canopy spectral invariants for remote sensing and model applications. *Remote Sensing of Environment*, *106*, 106–122.

Huang, D., Knyazikhin, Y., Yang, W., Deering, D. W., Stenberg, P., Shabanov, N. V., et al. (2008). Stochastic transport theory for investigating the three-dimensional canopy structure from space measurements. *Remote Sensing of Environment*, *112*, 35–50.

Justice, C. O., & Townshend, J. R. G. (2002). Special issue on the moderate resolution imaging spectroradiometer (MODIS): a new generation of land surface monitoring. *Remote Sensing of Environment*, *83*, 1–2.

Knyazikhin, Y., Martonchik, J. V., Myneni, R. B., Diner, D. J., & Running, S. W. (1998). Synergistic algorithm for estimating vegetation canopy leaf area index and fraction of absorbed photosynthetically active radiation from MODIS and MISR data. *Journal of Geophysical Research*, *103*, 32257–32274.

Knyazikhin, Y., Kranigk, J., Myneni, R. B., Panfyorov, O., & Gravenhorst, G. (1998). Influence of small-scale structure on radiative transfer and photosynthesis in vegetation cover. *Journal of Geophysical Research*, *103*(D6), 6133–6144.

Knyazikhin, Y., & Marshak, A. (2000). Mathematical aspects of BRDF modeling: adjoint problem and Green's function. *Remote Sensing Reviews*, *18*, 263–280.

Lavrentiev, M. M. (1967). *Some Improperly Posed Problems of Mathematical Physics*.New York: Springer-Verlag 72 pp.

Lewis, P., & Disney, M. (2007). Spectral invariants and scattering across multiple scales from within-leaf to canopy. *Remote Sensing of Environment*, *109*, 196–206.

Min, Q. (2005). Impacts of aerosols and clouds on forest-atmosphere carbon exchange. *Journal of Geophysical Research*, *110*, D06203. doi:10.1029/2004JD004858

Murphy, R. E. (2006). The NPOESS preparatory project. Earth Science Satellite Remote Sensing. *Springer Berlin Heidelberg*, 182–198. doi:10.1007/978-3-540-37293-6

Myneni, R. B., Keeling, C. D., Tucker, C. J., Asrar, G., & Nemani, R. R. (1997). Increased plant growth in the northern high latitudes from 1981–1991. *Nature*, *386*, 698–701.

Potter, C. S., Randerson, J. T., Field, C. B., Matson, P. A., Vitousek, P. M., Mooney, H. A., et al. (1993). Terrestrial ecosystem production: a process model based on global satellite and surface data. *Global Biogeochemical Cycles*, *7*(4), 811–841.

Sellers, P. J., Randall, D. A., Collatz, G. J., Berry, J. A., Field, C. B., Dazlich, D. A., et al. (1996). A revised land surface parameterization (SiB2) for atmosphere GCMs. Part II : The generation of global fields of terrestrial biophysical parameters from satellite data. *Journal of Climate*, *9*, 706–737.

Shabanov, N. V., Knyazikhin, Y., Baret, F., & Myneni, R. B. (2000). Stochastic modeling of radiation regime in discontinuous vegetation canopy. *Remote Sensing of Environment*, *74*, 125–144.

Shabanov, N. V., Huang, D., Yang, W., Tan, B., Knyazikhin, Y., Myneni, R. B., et al. (2005). Optimization of the MODIS LAI and FPAR algorithm performance over broadleaf forests. *IEEE Transactions in Geoscience and Remote Sensing*, *43*, 1855–1865.

Shabanov, N. V., Huang, D., Knyazikhin, Y., Dikinson, R. E., & Myneni, R. B. (2007). Stochastic radiative transfer model for mixture of discontinuous vegetation canopies. *Journal of Quantitative Spectroscopy & Radiative Transfer*, *107*, 236–262.

Smolander, S., & Stenberg, P. (2003). A method to account for shoot scale clumping in coniferous canopy reflectance models. *Remote Sensing of Environment*, *88*, 363–373.

Smolander, S., & Stenberg, P. (2005). Simple parameterizations for the radiation budget of uniform broadleaved and coniferous canopies. *Remote Sensing of Environment*, *94*, 355–363.

Steltzer, H., & Welker, J. M. (2006). Modeling the effect of photosynthetic vegetation properties on the NDVI-LAI relationship. *Ecology*, *87*(11), 2765–2772.

Tan, B., Hu, J., Zhang, P., Huang, D., Shabanov, N. V., Weiss, M., et al. (2005). Validation of MODIS LAI product in croplands of Alpilles, France. *Journal of Geophysical Research*, *110*, D01107. doi:10.1029/2004JD004860

Tan, B., Woodcock, C. E., Hu, J., Zhang, P., Ozdogan, M., Huang, D., et al. (2006). The impact of gridding artifacts on the local spatial properties of MODIS data: Implications for validation, compositing, and band-to-band registration across resolutions. *Remote Sensing of Environment*, *105*, 98–114.

Tian, Y., Wang, Y., Zhang, Y., Knyazikhin, Y., Bogaert, J., & Myneni, R. B. (2002). Radiative transfer based scaling of LAI/FPAR retrievals from reflectance data of different resolutions. *Remote Sensing of Environment*, *84*, 143–159.

ARTICLE IN PRESS

Tian, Y., Dickinson, R. E., Zhou, L., Zeng, X., Dai, Y., Myneni, R. B., et al. (2004). Comparison of seasonal and spatial variations of LAI/FPAR from MODIS and Common Land Model. *Journal of Geophysical Research*, *109*, D01103. doi:10.1029/2003JD003777

Tikhonov, A. N., Goncharsky, A. V., Stepanov, V. V., & Yagola, A. G. (1995). *Numerical Methods for the Solution of Ill-Posed Problems* (pp. 3). Boston: Kluwer Academic Publisher.

Tucker, C. J., Pinzon, J. E., Brown, M. E., Slayback, D. A., Pak, E. W., Mahoney, R., et al. (2005). An extended AVHRR 8-km NDVI data set compatible with MODIS and SPOT vegetation NDVI data. *International Journal of Remote Sensing*, *26*(20), 4485–5598.

Van Leeuwen, W. J. D., Orr, B. J., Marsh, S. E., & Herrmann, S. M. (2006). Multi-sensor NDVI data continuity: uncertainties and implications for vegetation monitoring applications. *Remote Sensing of Environment*, *100*, 67–81.

Vermote, E. F., & Saleous, N. Z. (2006). Calibration of NOAA16 AVHRR over a desert site using MODIS data. *Remote Sensing of Environment*, *105*, 214–220.

Wang, Q., Adiku, S., Tenhunen, J., & Granier, A. (2004). On the relationship of NDVI with leaf area index in a deciduous forest site. *Remote Sensing of Environment*, *94*, 244–255.

Wang, Y., Buermann, W., Stenberg, P., Voipio, P., Smolander, H., Häme, T., et al. (2003). A new parameterization of canopy spectral response to incident solar radiation: case study with hyperspectral data from pine dominant forest. *Remote Sensing of Environment*, *85*, 304–315.

Wang, Y., Tian, Y., Zhang, Y., El-Saleous, N., Knyazikhin, Y., Vermote, E., et al. (2001). Investigation of product accuracy as a function of input and model uncertainties: case study with SeaWiFS and MODIS LAI/FPAR algorithm. *Remote Sensing of Environment*, *78*, 296–311.

Yang, W., Shabanov, N. V., Huang, D., Wang, W., Dickinson, R. E., Nemani, R. R., et al. (2006). Analysis of leaf area index product from combination of MODIS Terra and Aqua data. *Remote Sensing of Environment*, *104*, 297–312.

Zhou, L., Tucker, C. J., Kaufmann, R. K., Slayback, D., Shabanov, N. V., & Myneni, R. B. (2001). Variations in northern vegetation activity inferred from satellite data of vegetation index during 1981 to 1999. *Journal of Geophysical Research*, *106*, 20069–20083.

WWW1: NOAA KLM User's Guide, Appendix D.2. http://www2.ncdc.noaa.gov/docs/klm/html/d/app-d2.htm#fd2-1

WWW2: MODIS Characterization Support Team (MCST), L1B Relative Spectral Response LUT. http://www.mcst.ssai.biz/mcstweb/index.html

Please cite this article as: Ganguly, S., et al., Generating vegetation leaf area index earth system data record from multiple sensors. Part 1: Theory, *Remote Sensing of Environment* (2008), doi:10.1016/j.rse.2008.07.014